Paper No. 1093. (quote when citing this article)
Eleventh World Conference on Earthquake Engineering
ISBN: 0 08 042822 3

CYCLIC STRENGTH AND STABILITY OF CLAY SUBJECTED TO INITIAL SHEAR STRESS

Masayuki HYODO
Department of Civil Engineering, Yamaguchi University, Ube 755, Japan
Yoichi YAMAMOTO
Technical Research Institute, Mitsui Construction Co. Ltd.,
518–1, Komaki, Nagareyama, Chiba 270–01, Japan
Teruhisa FUJII
Fukken Co. Ltd., Hikari–cho, 2–10–1, Higashi–ku, Hiroshima 732, Japa

ABSTEACT

A series of undrained cyclic triaxial tests has been performed on a plastic marine clay for normally consolidated condition in this study. Testing was carried out under various combinations of initial static and cyclic shear stresses. The cyclic shear strength is first considered, and then, the cumulative shear strain is investigated related to the effective stress ratio at the peak cyclic stress. Based on the experimental results, a semi–empirical model for predicting pore pressure and residual shear strain of clay developed during cyclic loading is proposed which will be a useful tool for practical design methods.

KEY WORDS

Clay; Cyclic loading; Cyclic triaxial test; Earthquake; Empirical model; Initial shear stress; Permanent strain; Pore pressure; Stability analysis.

INTRODUCTION

In considering earthquake design problems, interest has focused on the liquefaction of saturated sands. During earthquakes, clays have been considered to be stable in comparison with sands. Serious damage to structures sited on thick clay layers, however, was reported in the 1985 Mexico Earthquake (Seed et al. 1987, Mendoza et al., 1987). Additionally, many fill collapses were caused in Japan due to the failure of clay base layers in the 1964 Niigata Earthquake, 1978 Miyagiken–oki Earthquake (Sasaki et al. 1980) and 1983 Nihonkai– chuubu Earthquake. Such case histories from the previous earthquakes raise the question of whether or not clays are really more stable than sands during earthquakes. A comparison between the cyclic strengths for sand and clay has been made using laboratory tests, such as cyclic triaxial tests on isotropically consolidated specimens which simulate the horizontal layers. In this condition, clay may exhibit stability and the pore pressure in the clay may not develop up to the initial effective confining stress. Practically, however, most designs have been concerned with the base subsoils below structures or elements in slopes whose soil elements are generally subjected to the initial static shear stresses. A series of undrained cyclic triaxial tests were performed on a plastic marine clay for this study. Testing was carried out for various combinations of initial static and cyclic shear stresses which are those expected on soil elements subjected to cyclic loading in the vicinity of structures. Based on the experimental results, a semi–empirical model for predicting pore pressure and residual shear strain developed during cyclic loading is proposed which will be a useful tool for practical design methods.

TESTING PROCEDURE

Cyclic triaxial compression tests were carried out on remoulded Itsukaichi clay, a marine clay sampled from a depth of 8~10m below the seabed at Itsukaichi harbour, on the southwest coast of Hiroshima in Japan. Its index properties are G_s=2.532, w_L=124.2%, w_p=51.4% and I_p=72.8. In order to prepare the remoulded sample, the clay slurry mixed with an initial water content of 260% was poured into a consolidation vessel and was then preconsolidated with a vertical pressure of 50kPa. The specimens with initial dimensions of 50mm diameter and 100mm height were trimmed from the clay block. In order to obtain a high degree of saturation, a back pressure of 100kPa was applied for 1 hour. B-values of more than 0.97 were observed in all specimens used in the tests. To reduce the effect of friction on the clay behaviour during the test, two thin rubber sheets coated with silicone grease were placed between the lower and upper porous stones and the specimen and a hole 3mm in diameter made at the center of the lower membrane. Pore pressure was measured through the porous stone 3mm in diameter in the center of the lower pedestal. To accelerate consolidation a filter paper side drain was placed along the circumference of the sample to cover about 40%. Drainage occurred through the filter paper surrounding the specimen which was attached to the side of both porous stones. Normally consolidated specimens were initially consolidated isotropically and after a period of 24 hours consolidated anisotrpically by applying a static deviator stress at a constant mean principal stress of 200kPa in the triaxial cell.

A sinusoidal cyclic axial load was applied at a frequency of 0.02Hz, which was determined after investigating the homogeneity of the generation of pore pressures in specimens under undrained cyclic loading. Stress parameters p and q are used to represent the effective mean principal stress, $p=(\sigma_a'+2\sigma_r')/3$, and deviator stress, $q=\sigma_a'-\sigma_r'$, respectively. The symbols σ_{ic}' and p_c represent the lateral pressure and the value of p after consolidation, respectively in which σ_a' and σ_r' are axial and lateral stresses. Cyclic loading tests were performed over a range of initial static deviator stress ratio q_s/p_c varying from 0 to 1.2 at 0.3 intervals. From three to four magnitudes of cyclic deviator stress q_{cyc} were combined with each static deviator stress level so that both reversal and non-reversal of cyclic shear stresses were simulated.

CYCLIC BEHAVIOUR OF ISOTROPICALLY AND ANISOTROPICALLY CONSOLIDATED CLAY

Cyclic triaxial tests were performed using both reversal and non-reversal of cyclic shear stresses. Typical effective stress paths during cyclic loading for normally consolidated clay for each loading pattern are presented in Fig.1. The failure envelopes obtained from undrained monotonic tests on isotropically consolidated specimens are also drawn in each figure. The slopes of the envelopes for compression and extension are M_c=1.560 and M_e=1.456, respectively. In the isotropically consolidated case, as shown in Fig.1 (a), the effective stress path moved towards the failure envelopes during cyclic loading and finally traced a steady loop which reached the failure envelopes for both the compression and extension sides. Pore pressure measured at the bottom of the specimen through the pedestal did not develop up to the initial confining stress. In the anisotropically consolidated results, as shown in Fig.1 (b) the effective stress path moved until their upper part intersected the failure line on the compression side.

Typical results demonstrating the relationship between cyclic deviator stress and axial strain are presented in Fig.2. Smoothly expanding stress-strain hysteresis curves appeared for the isotropically consolidated clay as shown in Fig.2 (a). In the case of stress reversal from the compression to the extension side in the results presented in Figs.2 (a), significant magnitude of strain amplitude developed near the failure stage of cyclic loadings while in the non-reversal case, as illustrated in Fig.2 (b) residual strain was predominant instead of the cyclic component. Furthermore, it should be noted that an increase in the residual strain of clay during a cycle was triggered at the final stage of cycling when the stress paths approached the critical state line.

EVALUATION OF CUMULATIVE AXIAL STRAIN DURING CYCLIC LOADING

Attempts were made to quantify the accumulated axial strain corresponding to the peak cyclic stress on the compression side for each loading cycle. The peak axial strains ε_p from all tests were compared using an effective stress ratio η_p ($=q_s/p$) which is mobilized during cyclic loading and represents the ratio of the peak deviator stress divided by the corresponding mean effective principal stress at the peak value. The schematic diagram for presenting η_p at an arbitrary number of cycles and the corresponding ε_p is illustrated in Fig.3. Fig.4 presents the relationship between peak axial strain ε_p and effective stress ratio η_p for cyclic tests on normally consolidated specimens. Although some scatter occurs, generally in the figures, there is a unique relationship between peak axial strain and effective stress ratio although the magnitudes of initial static and applied cyclic deviator stresses are different from each other. Furthermore, it was found as shown in the figure that although

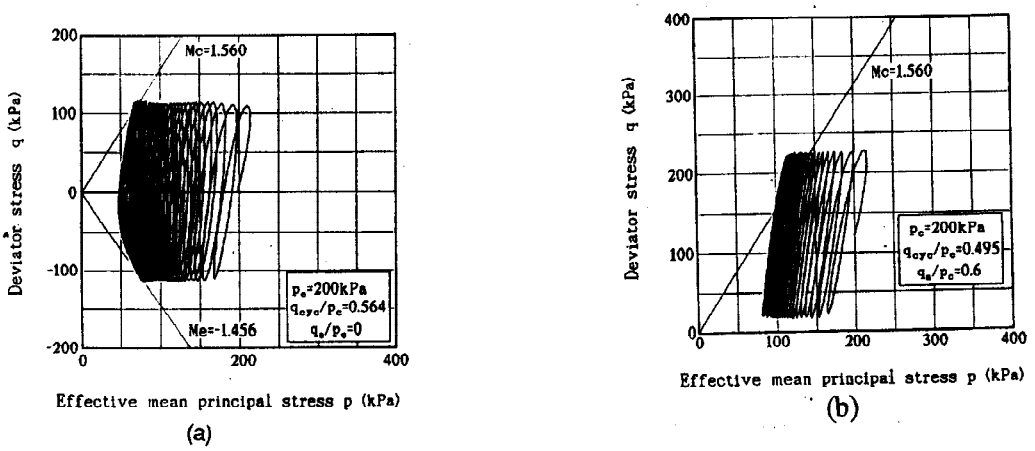

Fig.1 Effective stress paths in the cases of, (a): isotropically consolidated, (b): anisotropically consolidated

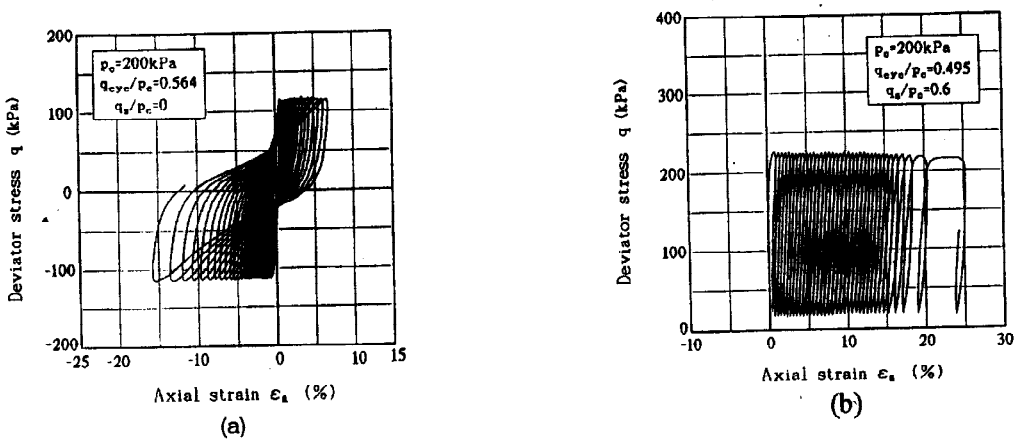

Fig.2 Relationships between deviator stress and axial strain in the cases of, (a):isotropically consolidated, (b):anisotropically consolidated

the starting points are different for each initial static deviator stress, most of the relationship can be approximated by a unique hyperbola given by the following equation.

$$\varepsilon_p = a_1 \eta_p / (1 - \eta_p / \eta_{ult}) \quad (1)$$

where $1/a_1$ means the slope of the initial tangential line of $\varepsilon_p - \eta_p$ curve and η_{ult} is the value of η at the asymptote of the hyperbola. The parameters were determined to be a_1=0.5 and η_{ult}=2.0 based on these results, respectively. A similar relationship was also observed in anisotropically consolidated sand (Hyodo et al. 1991).

CYCLIC SHEAR STRENGTH

It is convenient to make a unified definition of cyclic shear strength for both reversal and non-reversal stress conditions. In the relationship shown in Fig.4, the cyclic failure is defined as the peak accumulated axial strain ε_p=10% because the hyperbola shown in this figure approaches asymptotically at about ε_p=10%. Considering this failure criterion for both the reversal and non-reversal regions, the relationship between the cyclic deviator stress ratio and the number of cycles required to cause failure for each initial static deviator stress q_s is represented as shown in Fig.5. The cyclic strength for the clay with zero initial static deviator stress ratio was determined to be 10% of the double amplitude of axial strain, DA instead of ε_p although it is not certain whether both failure criteria are equivalent to each other or not. It can be observed in this figure that the cyclic shear strength for clay decreases with increasing initial static deviator stress. In order to compare the cyclic shear strength for clay with that for sand, the cyclic shear strength curves for isotropically consolidated clay and Toyoura sand with Dr=50% and 70% (Hyodo et al. 1991) are presented in Fig.6. In the isotropically consolidated condition, the cyclic strength

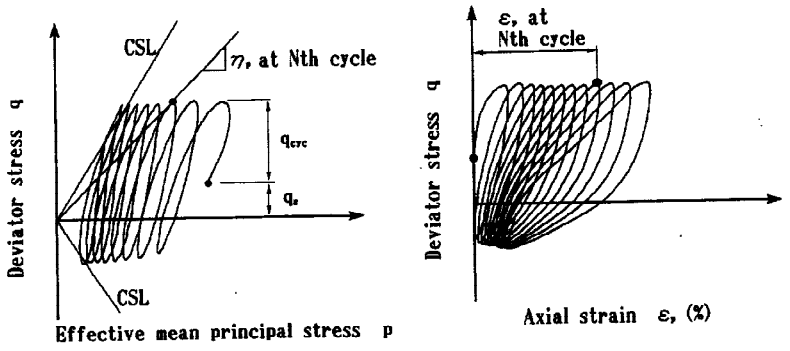

Fig.3 Schematic diagram for peak axial strain ε_p and corresponding effective stress ratio η_p at an arbitrary cycle during cyclic loading

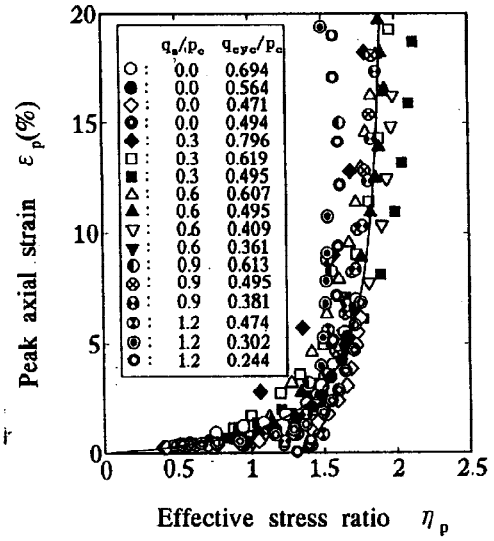

Fig.4 Relationship between peak axial strain ε_p and effective stress ratio η_p at each cycle during cyclic loading

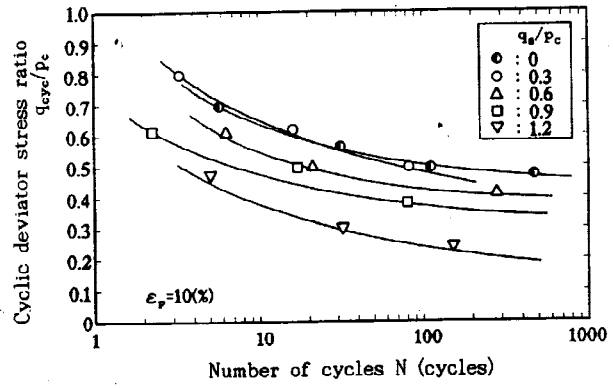

Fig.5 Relationship between cyclic deviator stress ratio q_{cyc}/p_c and number of cycles to cause peak axial strain ε_p=10%

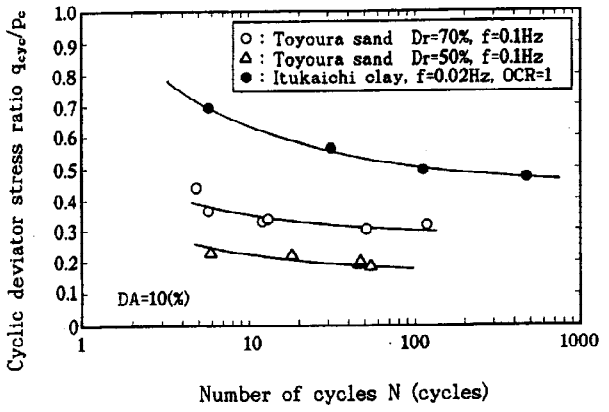

Fig.6 Relationship between cyclic deviator stress ratio q_{cyc}/p_c and number of cycles to cause double amplitude of axial strain DA=10%

for clay is about two or three times as high as that for sand.

The variations of cyclic deviator stress ratio required to cause ε_p=10% in 20 cycles with initial static deviator stress ratio for both clay and sand are summarized in Fig.7. It can be seen in both of these figures that the cyclic deviator stress ratio to cause failure in clay decreases with increasing initial static deviator stress. Cyclic shear strength for sand increases with increasing initial deviator stress. In the isotropically consolidated condition, the cyclic strength for clay is certainly greater than that for sand. The inequality is reversed however at a certain initial static deviator stress. Especially in the non-reversal region, cyclic shear strength for clay is far lower than that for sand. It appeared therefore that the clay subjected to initial static shear stress, such as a layer upon which the structure is founded, is more unstable than sand during cyclic loading. This result is caused by the fact that intermediate dense to dense sands increase undrained strengths due to positive dilatancy on approaching failure (Hyodo et al., 1991); on the other hand, approaching to critical state, clays show the characteristics to decrease strength and to increase deformation. Judging from the fact, clayey deposits should be examined the stability against cyclic shear failure especially for foundations of structures. The schematic diagrams explaining the difference of seismic failure modes between clay and sand deposits are represented in Figs.8(a) and (b). The figures show that seismic failure of clay deposit occurs in the visinity of the the structure due to the large initial shear stress and

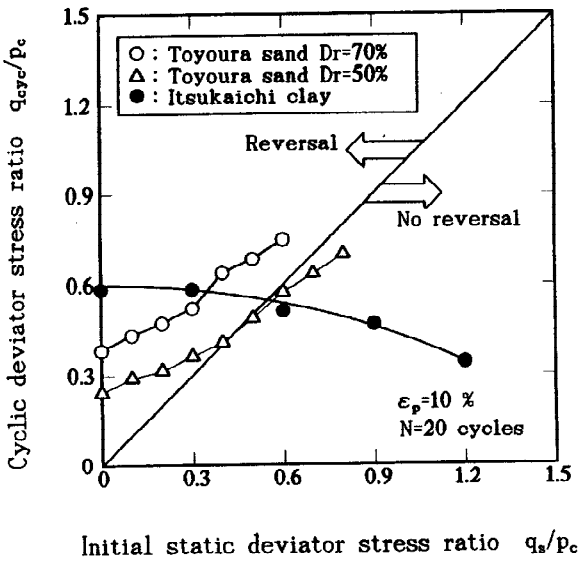

Fig.7 Relationship between normalized cyclic deviator stress and initial static deviator stress to cause ε_p=10% at 20 cycles for clay and sand

large inertia force of structure because the it still remains the effective stress at the failure condition while that of sand deposit is due to the liquefaction of whole base layer followed by the loss of the effective stress.

For the purpose of development of the empirical model, redefining the cyclic strength as $R_f=\{(q_{cyc}+q_s)/p_c\}_f$ where substrict f means the state of failure, it can be approximated by straight lines in logarithmic form. These are parallel straight lines for each initial static deviator stress as shown in Fig.9 in which the cyclic strength for $q_s/p_c=0$ is also illustrated and formulated by the following equation:

$$R_f=\{(q_{cyc}+q_s)/p_c\}_f = \kappa N^{\beta} \tag{2}$$

where β is slope of each strength line given by $\beta=-0.088$ and κ is cyclic strength for the first cycle which is related by normalized initial deviator stress as $\kappa=0.771+1.157q_s/p_c$.

RELATIVE EFFECTIVE STRESS RATIO AND CYCLIC SHEAR STRESS

In the previous section of this paper, a unified cyclic shear strength, $R_f=\{(q_{cyc}+q_s)/p_c\}_f$, applicable to all the loading patterns was defined. In order to represent the undrained cyclic behaviour of clay, the following two parameters are introduced. The first parameter is defined as an index of the possibility of cyclic failure, $RR(N)=R/R_f$ which is the ratio of the peak cyclic deviator stress, $R=(q_s+q_{cyc})/p_c$, to the cyclic shear strength, $R_f=\{(q_{cyc}+q_s)/p_c\}_f$ in a given number of cycles. RR(N), named relative cyclic shear stress, whose schematic diagram is shown in Fig.10, is equivalent to the reciprocal of the safety factor against cyclic failure. When the magnitude of R is constant, $RR(N)=R/R_f$ increases with increasing number of cycles and varies from zero at non-loading to unity at failure.

The second parameter is defined as:

$$\eta^* = (\eta_p - \eta_s)/(\eta_f - \eta_s) \tag{3}$$

where η_p is the effective stress ratio at the peak of the cyclic stress in each cycle, η_s is the effective stress ratio for initially consolidated conditions and η_f is the effective stress ratio at failure. This parameter, η^*, therefore, indicates the relative effective stress ratio between the initial point and the final point in p-q space as shown in Fig.11. These parameters were originally introduced for sand by Hyodo et al. (1991) and also applied to isotropically and anisotropically consolidated clays (Hyodo et al. 1992, 1994). By correlating the values of both parameters, we obtain Fig.12 for each q_s/p_c. Despite the difference in initial static and subsequent cyclic deviator stresses, the best fit curve for each relation is given by a unique curve formulated by the following equation:

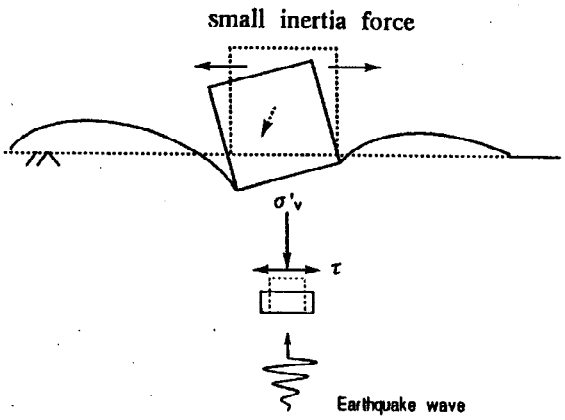

(a):liquefaction of sand

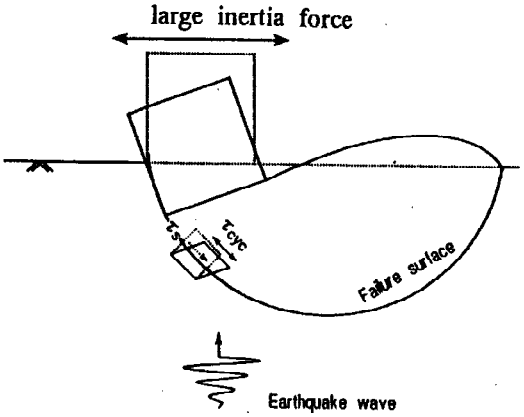

(b):cyclic shear failure of clay

Fig.8 Comparison between liquefaction of sand and cyclic shear failure of clay
(a):liquefaction of sand,
(b):cyclic shear failure of clay

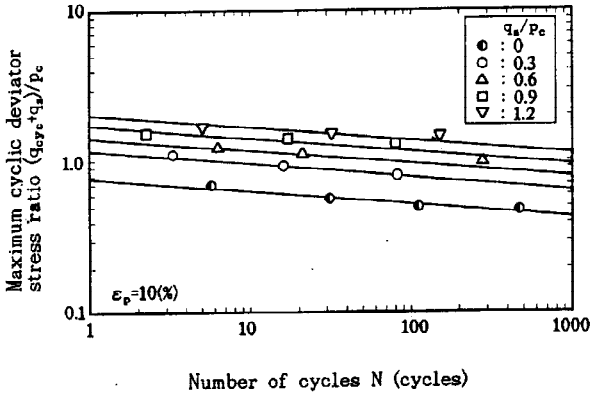

Fig.9 Relationship between cyclic deviator stress ratio $(q_s+q_{cyc})/p_c$ and number of cycles to cause peak axial strain ε_p=10%

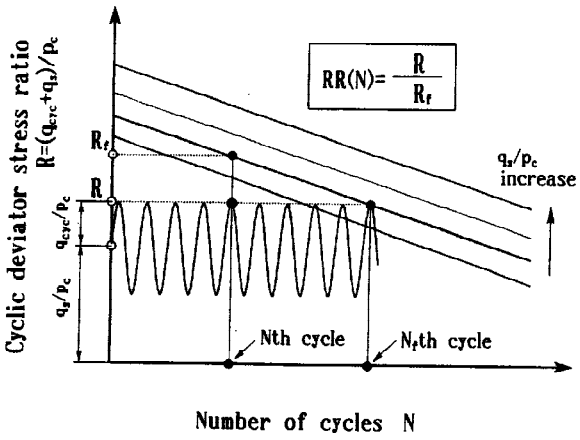

Fig.10 Schematic diagram for relative cyclic shear stress RR(N)

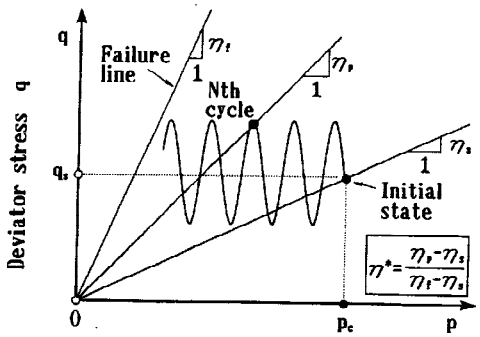

Fig.11 Schematic diagram for relative effective stress ratio $\eta^*=(\eta_p-\eta_s)/(\eta_f-\eta_s)$

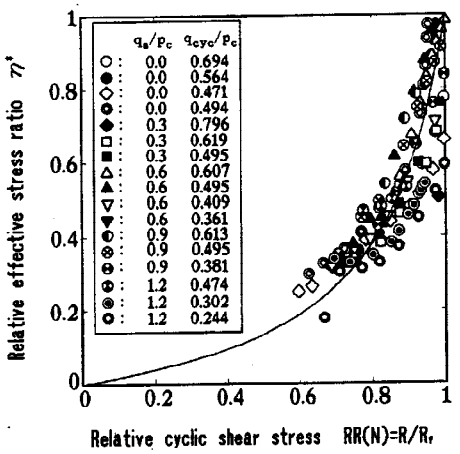

Fig.12 Relationship between relative effective stress ratio η^* and relative cyclic shear stress ratio RR(N)=R/R_f

$$\eta^* = R/R_f/\{a_2-(a_2-1)R/R_f\} \quad (4)$$

where a_2 was determined as 6.5.

Cyclic-induced peak axial strain is calculated using the following procedure:
(1) The cyclic shear strength R_f for the desired initial static deviator stress and number of stress cycles is determined from the relationship given by Eq.(2). Then the relative cyclic shear stress R/R_f is obtained by dividing the applied stress ratio R by the strength R_f.

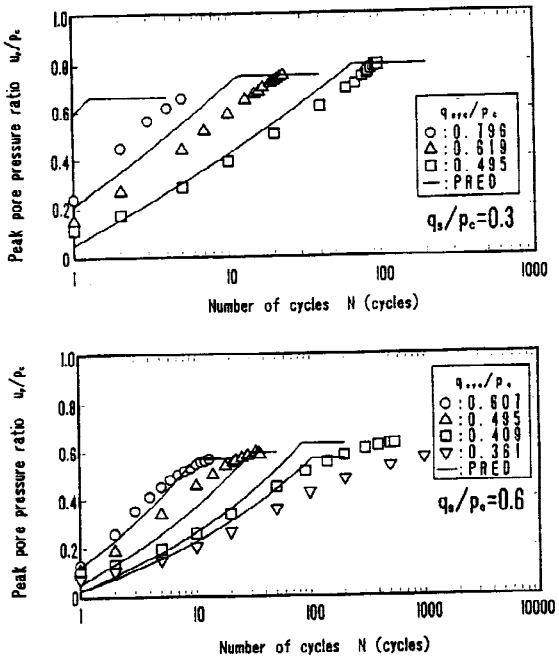

Fig.13 Predicted and experimental pore pressurer at the peak cyclic stress

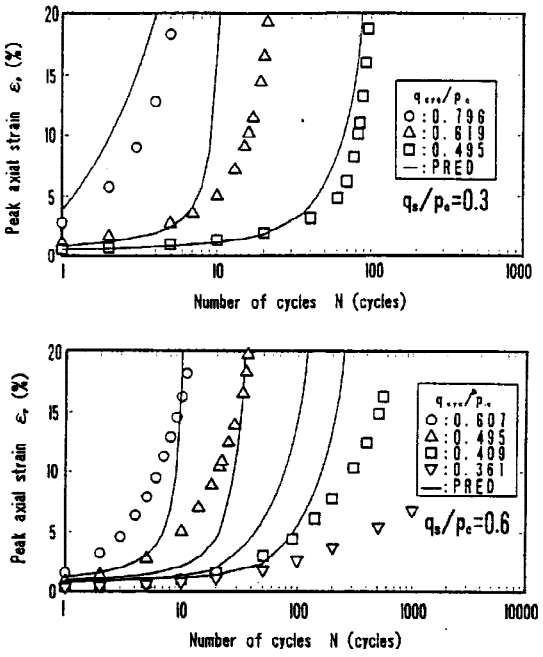

Fig.14 Predicted and experimental accumulated peak axial strain

$$\eta^* = R/R_f/\{a_2-(a_2-1)R/R_f\} \tag{4}$$

where a_2 was determined as 6.5.

Cyclic-induced peak axial strain is calculated using the following procedure:
(1) The cyclic shear strength R_f for the desired initial static deviator stress and number of stress cycles is determined from the relationship given by Eq.(2). Then the relative cyclic shear stress R/R_f is obtained by dividing the applied stress ratio R by the strength R_f.
(2) The relative effective stress ratio η^* is obtained by substituting R/R_f into the relationship between η^* and R/R_f given by Eq.(4).
(3) The effective stress ratio η_p at the peak cyclic stress of a given stress cycle is calculated by the following rewritten form of Eq.(3).

$$\eta_p = \eta^*(\eta_f - \eta_s) + \eta_s \tag{5}$$

(4) The pore pressure at the peak axial strain is calculated substituting η_p into the following equation.

$$u_p = p_c + q_{cyc}/3 - (q_s + q_{cyc})/\eta_p \tag{6}$$

(5) The peak axial strain is evaluated by substituting η_p into Eq.(1).

If these steps are repeated from the first to the last stress cycle, the accumulated peak pore pressures and peak axial strains can be predicted for the number of cycles during cyclic loading. The predicted and observed pore pressures and axial strains are presented in Figs.13 and 14 in which the results for each initial static and subsequent cyclic shear stresses are illustrated. In these figures, the predicted and observed results correspond to solid lines and plots, respectively.

Fairly good correspondence is recognized between the predicted and experimental results in spite of very complicated initial conditions. It was confirmed that the proposed model is a reasonable method for accumulating the cyclic-induced pore pressure and shear strain of clay subjected to various magnitudes of initial static and subsequent cyclic shear stresses.

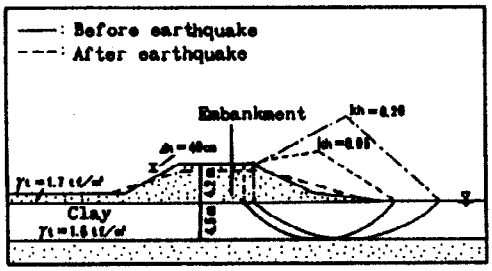

Fig.15 Transverse section of the dike alog the Yoshida River

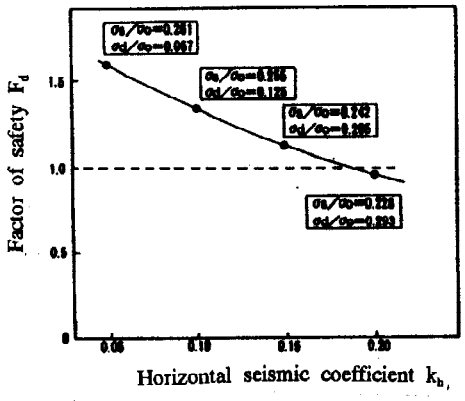

Fig.16 $F_d \sim k_h$ relation for the Yoshida River dike

SEISMIC STABILITY ANALYSIS FOR EMBANKMENT FOUNDED ON CLAYEY DEPOSIT

The case history for seismic damage was analyzed with paying attention to clayey deposit and the seimic failure mode shown in Fig.8(a). The cyclic strength of clay subjected to initial shear stress is evaluated from Eq.(2) ($R_f=\{(q_{cyc}+q_s)/p_c\}_f = \kappa N^{\beta}$) which is dependent on the magnitude of initial shear stresses.

The embankment analyzed here is the dike along the Yoshida River which was collapsed during the Niigata Earthquake 1964. The soil profile beneath dike was a soft clay deposit about 5m with N-value of 0 to 1 laid over a sand deposit with N-value over 5. The ground water level was located at near ground surface. This dike was destroyed completely in soft saturated clay layer during the earthquake to occur the settlement of about 40cm to 50cm at ground surface (Sasaki et al., 1980). Fig.15 shows the configuration of the transverse section of dike before and after the earthquake. The sliding circle shown in Fig.15 is the circle of minimum factor of safety for each seismic coefficient. The positions and radii of seismic sliding circle of minimum factor of safety are different depending on seismic coefficients. A tendency is seen from the analytical result that the position of circle shifts to the top of slope with increasing seismic coefficient. Fig.16 shows the calculated results corresponding to result is assessed to be valid judging from the seismic accelerogram of about 150gal to 200gal recorded during the earthquake. The position and radius of sliding circle show the good accordance with the sliding configuration expressed in the damage report for dike.

CONCLUSIONS

(1) The cyclic shear strength tended to decrease with inicreasing initial static shear stress. It was the opposite tendency from that for Toyoura sand. (2) A unique relationship was recognized between peak axial strain and mobilized effective stress ratio measured for each stress cycle during cyclic loading, despite various initial static and subsequent cyclic shear stresses. (3) We found that the new parameters, the relative effective stress ratio η^* and the relative cyclic shear stress, $RR(N)=R/R_f$ used in the present paper are uniquely correlated with each other. (4) By using the relationships noted in (3) and (4), it was possible to predict the accumulated pore pressure and peak axial strain of clay with initial static shear stress subjected to cyclic loading.
(5) Using the method of seismic stability analysis and the cyclic strength properties obtained from the cyclic triaxial tests, the analytical results reasonably agreed with the actual damage case histry.

REFERENCES

Hyodo, M., Murata, H., Yasufuku, N. and Fujii, T. (1991). Undrained cyclic shear strength and residual shear strain of saturated sand by cyclic triaxial tests, *Soils and Foundations*, Vol.31, No.3, pp.60–76.

Hyodo, M., Yasuhara, K. and Hirao K. (1992). Prediction of clay behaviour in undrained and partially drained cyclic triaxial tests, *Soils and Foundations*, Vol.32, No.4, pp,117–127.

Hyodo, M., Yamamoto, Y. and Sugiyama, M. (1994). Undrained cyclic shear behaviour of normally consolidated clay subjected to initial static shear stress, *Soils and Foundations*, Vol.34. No.4, pp.1–11.

Mendoza, M.J. (1987). Foundation Engineering in Mexico City: Behavior of Foundations, *Proc. of the Int. Symp. on Geotechnical Engineering Soft Soils*, Vol.2, pp.351–367.

Sasaki, Y., Taniguchi, E., Matsuo, O. and Tateyama, M. (1980). Damage of soil– structures by earthquakes, *Technical Note of PWRI*, No.1576, Public Works Research Institute, (in Japanese).

Seed, H.B., Romo, M.P, Sun, J.I., Jaime, A. and Lysmer, J. (1987). Relationships between soil conditions and earthquake ground motions in Mexico City in the Earthquake of September 19, 1985, *Report No.UCB/EERC–87/15. Univ. of California. Berkeley.*